Applied Surface Science 548 (2021) 149270

Contents lists available at ScienceDirect

Applied Surface Science

journal homepage: www.elsevier.com/locate/apsusc

Full Length Article

Adsorption of transition metal clusters on Boron-graphdiyne

Estefanía Germán *, Ana Alvarez-Yenes, Julio A. Alonso, María J. López

Departamento de Física Teórica, Atómica y Optica, University of Valladolid, 47011 Valladolid, Spain

ARTICLE INFO

Keywords:
Boron-graphdyine
Density functional theory
Metallic nanoparticles
Vanadium
Cobalt
Palladium

ABSTRACT

Layered carbon materials can be useful as supports for catalytic metallic nanoparticles in different applications. Also, doping porous carbons with metal atoms and nanoparticles enhances the hydrogen storage capacity of those materials. We have investigated the adsorption of transition metal atoms and small clusters on boron graphdiyne (BGDY) using density functional theory. This layered material contains uniformly distributed large hexagonal holes that can host the metal clusters. Single V, Co and Pd atoms sit at the hexagon corners, near the B atoms. Their binding energies are large enough to make the systems suitable for single-atom catalysis but atomic diffusion cannot be overlooked. Formation of dimers of those three elements near the hexagon corners is preferred over decoration by two separated atoms. The octahedral structure of the free hexamers is preserved on adsorption of V_6 and Co_6, but it changes in Pd_6. The adsorption sites of the three hexamers are different. The adsorption energies of single atoms, dimers and hexamers on BGDY are substantially larger than those on pristine graphene, and similar to those on graphdiyne, but the larger holes existing in BGDY make this system better tuned for some applications.

1. Introduction

Carbon feeds the basis for life on earth, and is found in almost all life forms. The four valence electrons ($2s^2$ $2p^2$) of the atom allow carbon to form different types of bonds with other carbon atoms, and also to form bonds with almost any chemical element. Carbon adopts several forms, such as graphite, diamond, lonsdaleite and different kinds of amorphous, glassy and porous structures [1]. Carbon nanostructures such as graphene, fullerenes, carbon nanotubes, nanorings, nanoribbons, and others, have become increasingly popular nowadays. The discovery of new carbon nanostructures with attractive properties like high stability, novel bonding characteristics, and new applications represents a constant effort in materials science.

After the successful isolation of graphene [2], the field of two-dimensional (2D) materials has enjoyed a rapid rise. Graphene is the best-known member of the family of 2D materials, showing exceptional properties [3,4], and these properties place graphene as a promising candidate for different applications [5] in nanoelectronics and nano-optics, in mechanically robust and stretchable nanodevices, etc. The exciting graphene properties have boosted the discovery, design and study of other layered materials based on carbon. One of those materials is graphdiyne (GDY) [6], a synthetic carbon allotrope with a structure which is a layered framework formed by benzoic rings connected by very stable carbon chains containing diacetylenic linkages. The structure of GDY presents an ordered arrangement of triangular holes in the planar layers. This special arrangement delivers electronic and optical properties [7] showing interesting differences compared to graphene, such as a band gap opening, high third-order nonlinear optical susceptibility and high fluorescence efficiency. The peculiar structure, and the electronic, optical and mechanical properties make GDY promising for applications in electrode materials [8], nanoelectronics [9], energy storage (hydrogen [10] and lithium storage [11]), gas separation [12] and others.

A new member in the GDY family is boron-graphdiyne (BGDY). In this 2D structure, single boron atoms replace the hexagonal carbon rings in the GDY lattice. Because boron has three valence electrons, the B atom forms bonds with three carbon butadiyne chains, leading to the formation of a 2D honeycomb lattice (see Fig. 1) with large hexagonal holes. BGDY was synthetized by a bottom-to-up strategy [13]. The work reporting the discovery of this material also explored its application in sodium storage. Theoretical methods have been employed by Mortazavi et al. [14] to study the mechanical, electronic and optical properties, and the thermal conductivity of single-layer BGDY. These authors and others [15] also explored the application of BGDY as an anode for alkaline and alkaline-earth ion batteries. Wang and coworkers [16] have calculated the electronic band structure of BGDY, showing that it is a

* Corresponding author.
E-mail address: estefania.german@uva.es (E. Germán).

https://doi.org/10.1016/j.apsusc.2021.149270
Received 7 October 2020; Received in revised form 29 December 2020; Accepted 6 February 2021
Available online 9 February 2021

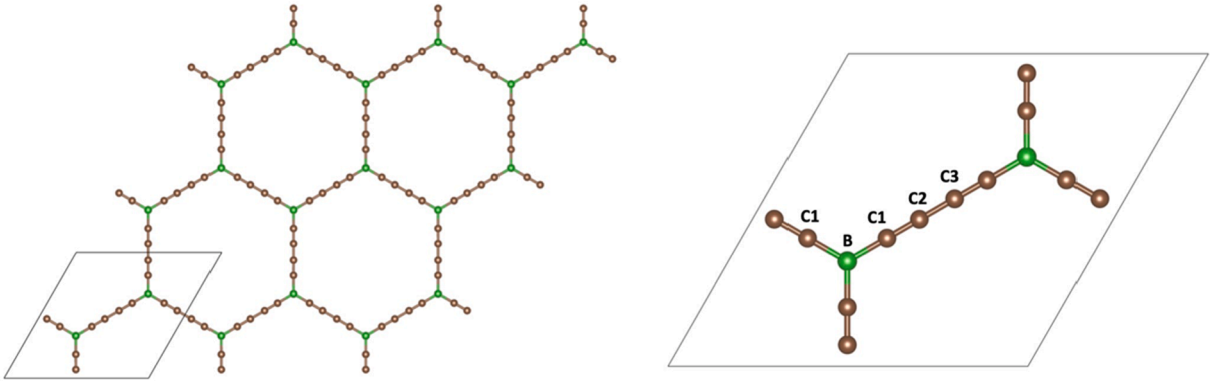

Fig. 1. Left panel: honeycomb structure of BGDY. Boron and carbon atoms are represented by green and brown spheres, respectively. Right panel: labelling of adsorption sites: on top B, on top C1, on top C2; C1-C2 bridge, C2-C3 bridge; in-plane C1-C2 bridge; C1-B-C1 corner. The carbon atoms are labelled by increasing distance to the B atom. (For interpretation of the references to colour in this figure legend, the reader is referred to the web version of this article.)

semiconductor with high electron and hole mobilities. Doped BGDY sheets with light metal atoms (Li, Na, K, Ca) were investigated by Hussain et al. [17] as hydrogen storage materials.

We present the results of a computational investigation of the adsorption of transition metal atoms and clusters on BGDY. The specific metals are vanadium, cobalt and palladium. Transition metal atoms and nanoparticles have been found to enhance the hydrogen storage capacity of porous carbons [18–20], and the same can be expected for GDY and BGDY. Also, layered carbon materials can serve as substrates for catalytic metal nanoparticles [21], and the structure and stability of the adsorbed nanoparticles is relevant in practice. Supported single-atom catalysts [22] are more selective and efficient than nanoparticles in specific reactions, and the stability of the adsorbed single atom against diffusion, desorption and aggregation becomes a crucial issue. Finding optimal support materials for both single-atom and nanoparticle catalysts will be of great help. In Section 2 we briefly present the method used to simulate the adsorption of atoms and clusters on a BGDY layer. Section 3 contains the analysis of the adsorption of single V, Co and Pd atoms on BGDY. Whenever possible, the adsorption on BGDY is compared with the adsorption on other carbon substrates. Adsorption of two atoms is discussed in Section 4, and it is found that formation of adsorbed dimers is energetically favorable against the configuration of two separated adsorbed atoms. Barriers for metal atom diffusion are discussed in Section 4. For larger clusters like the hexamer, discussed in Section 5, important questions are the optimal location of the clusters on the BGDY layer, and if the cluster structures changes or not on adsorption. Section 6 summarizes the conclusions.

2. Theoretical method and adsorption model

To determine the electronic and structural properties of transition metal atoms (M = V, Co and Pd) and their clusters adsorbed on BGDY, density functional theory calculations have been performed. We employed the quantum-ESPRESSO suite of electronic structure codes, version 6.4.1 [23]. The Perdew-Burke-Ernzerhof generalized gradient approximation (GGA-PBE) was selected for the exchange-correlation functional [24,25]. The electron-ion core interactions were modeled using the projected augmented wave method (PAW) [26,27]; namely, C.pbe-n-kjpaw_psl.1.0.0.UPF for carbon, B.pbe-n-kjpaw_psl.1.0.0.UPF for boron, V.pbe-spnl-kjpaw_psl.1.0.0.UPF for vanadium, Co.pbe-spn-kjpaw_psl.0.3.1.UPF for cobalt and Pd.pbe-n-kjpaw_psl.1.0.0.UPF for palladium. These pseudopotentials, available from the Quantum ESPRESSO Web site [28], correspond to the following electronic configurations: $2s^2\ 2p^2$ for C, $2s^2\ 2p^1$ for B, $3s^2\ 4s^2\ 3p^6\ 3d^3$ for V, $3s^2\ 4s^2\ 3p^6\ 3d^7$ for Co, and $4d^9\ 5s^1$ for Pd. This choice amounts to considering 4 external electrons for C, 3 for B, 13 for V, 17 for Co, and 10 for Pd. A cutoff energy of 45 Ry was selected for the plane waves used to expand the Kohn-Sham orbitals, and 350 Ry for the charge density. Higher cutoffs did not affect significantly the results. The Brillouin-zone was sampled with a 3 × 3 × 1 Monkhorst-Pack grid [29]. To account for dispersion corrections to the energy density functionals, the Grimme-D3 method was taken into account [30].

The BGDY layer was modeled using a repetitive cell containing 14 atoms (12 C atoms and 2 B atoms) and a vacuum spacing of 20 Å in the direction perpendicular to the layer (see Figs. 1 and 2). This cell is used

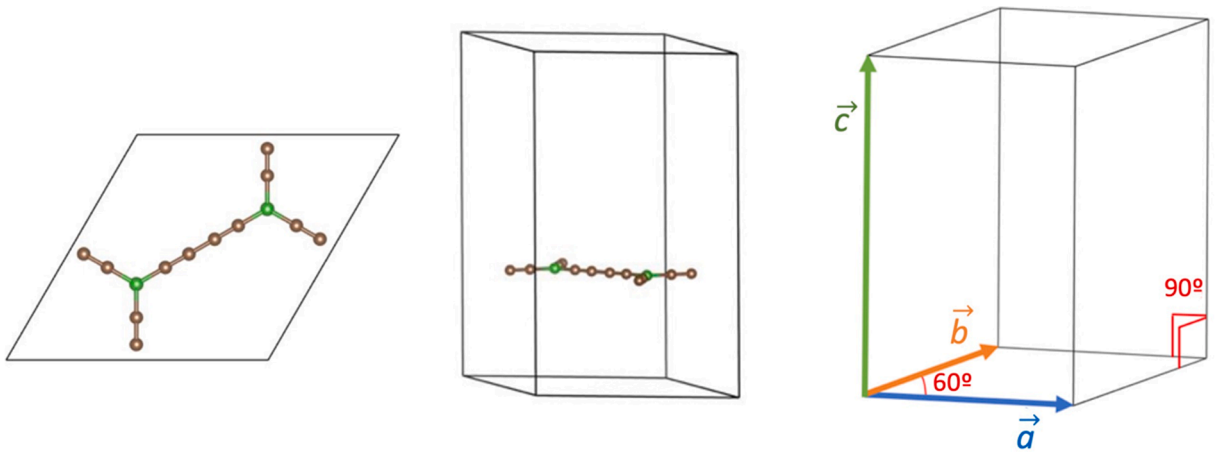

Fig. 2. Top and side views of the three-dimensional unit cell used in the calculations. On the right side panel, unit cell vectors and angles (a = b = 11.847 Å, c = 20 Å).

Table 1
Adsorption energies (in eV) of V, Co and Pd atoms on different sites of BGDY layer.

Sites	E_{ads} (V)	E_{ads}(Co)	E_{ads}(Pd)
On top B	2.36	–	–
On top C1	2.73	2.43	2.25
On top C2	–	2.03	–
Bridge C1-C2	–	–	2.25
Bridge C2-C3	2.84	–	–
Corner C1-B-C1	3.34	3.05	2.39
In-plane bridge C1-C2	3.01	2.00	–

to represent a crystalline BGDY layer and the layer doped with metal atoms and clusters. We have analyzed the possible adsorption sites for single V, Co and Pd atoms on the BGDY layer. In the case of clusters, isolated M_n structures (M = V, Co, Pd) were optimized and then adsorbed on the surface, and preferred adsorption regions and cluster geometries were optimized. Adsorption energies were computed as follows:

$$E_{ads}(M_n) = E(BGDY) + E(M_n) - E(M_n@BGDY). \quad (1)$$

E(BGDY), E(M_n) and E(M_n@BGDY) are the total energies of the clean BGDY cell, the isolated cluster having n atoms, and the system formed by the cluster adsorbed on the BGDY layer. According to this definition, a positive adsorption energy value corresponds to energetically favorable adsorption on the surface. The equation is also valid for the adsorption of a single atom (with n = 1). To investigate the possible decoration on BGDY, as opposed to clustering, we have compared the adsorption energy of a second M atom in the vicinity of the first pre-adsorbed M atom (clustering) and the adsorption energy on other sites on the surface far from this pre-adsorbed M atom (decoration). Full optimization of all the structures has been performed, allowing for possible deformations of the BGDY layer. Diffusion barriers between relevant adsorption sites have been calculated using the nudged elastic band method [31].

3. Single transition metal atoms on the BGDY surface

BGDY is a layered framework related to graphdiyne (GDY). It is formed by boron atoms connected by carbon chains containing diacetylenic −C≡C−C≡C− linkages. The layer structure, shown in Fig. 1, displays an ordered arrangement of hexagonal holes, with the two ends of the carbon chains (which form the hexagon sides) linked to the boron atoms. The periodic three-dimensional cell used in the calculations is shown in Fig. 2. First, the unit cell of single-layer BGDY, which contains two B atoms and twelve C atoms, was optimized. The optimized a and b lattice constants (see Fig. 2) are a = b = 11.847 Å. The calculated B–C bond length is 1.52 Å, close to that in boron-doped graphene (1.50 Å) [32], and the bond lengths of triple C≡C bonds and single C–C bonds are 1.23 Å and 1.36 Å, respectively, in agreement with previous work on GDY [33,34].

After optimizing the geometry and cell parameters of the BGDY monolayer, the adsorption energies of a single metal atom on different positions were calculated. Those positions can be viewed with the aid of Fig. 1: a) on top of the B atom, on top of C1 and C2 atoms; b) C1-C2 and C2-C3 bridges; c) in-plane bridge positions between C1 and C2 atoms; d) the C1-B-C1 corner. The carbon atoms are labelled by increasing distance to the B atom. The results are given in Table 1. Missing entries in the Table correspond to unstable positions; that is, the adsorbed metal atoms move to other more stable sites during the optimization of the structure. The most stable adsorption positions of the metal atoms are in the C1-B-C1 corners, with the metal atoms sitting above the layer, as can be seen in Fig. 3. The interaction with the adsorbed atoms induces the local distortion of the BGDY layer, and the deviation from layer planarity is larger for V as compared to Co and Pd. Adsorption energies (see Table 1) are 3.34, 3.05 and 2.39 eV for V, Co and Pd, respectively. The trend in adsorption energies correlates with the amount of bonding charge

$$\Delta\rho(\mathbf{r}) = \rho[M@BGDY](\mathbf{r}) - \rho[M](\mathbf{r}) - \rho[BGDY](\mathbf{r}), \quad (2)$$

which is plotted and discussed in the Supplementary Material.

The distances between the metal atoms and the neighbor atoms of the BGDY layer are given in Table 2. The distance to the boron atom, d(M-B), is shorter for Co, as compared to V and Pd, and as a consequence also the distances from Co to the C1 atoms, d(M-C1), and to the C2 atoms, d(M-C2), of that specific corner are smaller than the corresponding distances for V and Pd atoms. This trend correlates with the

Table 2
Interatomic distances (in Å) between: 1) the adsorbed metal atom and the B atom, d(M-B), in M@BGDY; 2) the adsorbed metal atom and the two nearest C atoms of the corner, d(M-C1); 3) the adsorbed metal atom and the third and fourth nearest C atoms, d(M-C2). Metal atoms sit in the corner adsorption site (see Figs. 1 and 3).

Distances	V-BGDY	Co-BGDY	P-BGDY
d(M-B)	2.285	2.178	2.249
d(M-C1)	2.140; 2.053	1.915; 1.890	2.146; 2.150
d(M-C2)	2.592; 2.198	2.254: 2.141	2.708; 2.726

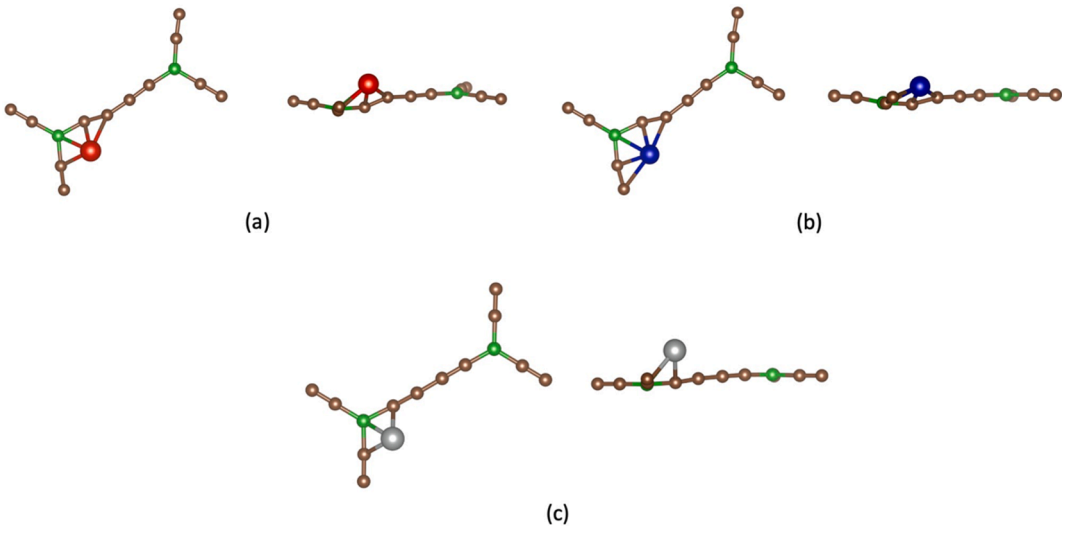

Fig. 3. Top (left) and side (right) views of the most stable adsorption geometries for (a) vanadium, (b) cobalt and (c) palladium atoms on BGDY.

Table 3
Adsorption energy E_{ads} (in eV) and magnetic moment μ (in μ_B) of a Pd atom, a dimer Pd_2, and the hexamer Pd_6, on different substrates: graphene, graphene vacancy, graphdiyne, and boron-graphdiyne. E_{ads} is calculated from Eq. (1). The magnetic moments of the isolated species are also included.

	Single atom		Dimer		Hexamer	
Configuration	E_{ads}	μ	E_{ads}	μ	E_{ads}	μ
Free (this work)		0		2		2
Free [35]		0		2		2
On graphene [36,37]	1.08–1.09	0	1.26	0	1.14	2
On graphene vacancy [38]	5.13	0	5.93	0	5.62	0
On GDY [34]	2.54	0	3.74	0	3.97	0
On BGDY (this work)	2.39	0	3.54	0	4.21	0

Table 4
Adsorption energy E_{ads} (in eV) of M, M_2 and M_6 (M = V, Co, Pd) on BGDY. E_{ads} has been calculated from Eq. (1). Also, magnetic moment per cell, μ (in μ_B).

	V		Co		Pd	
	E_{ads}	μ	E_{ads}	μ	E_{ads}	μ
Single atom	3.34	3	3.05	1	2.39	0
Dimer	4.00	0	3.33	2.69	3.54	0
Hexamer	6.26	2	4.12	10	4.21	0

magnitude of the atomic radius of the metal atoms.

A comparison of the adsorption energies of a single Pd atom on different carbon substrates is shown in Table 3. The binding energies of a Pd atom on BGDY and GDY are similar, and substantially higher than the binding energy on pristine graphene. The binding energies of V and Co atoms on graphene have been calculated by Valencia and coworkers [39]. The values $E_{ads}(V) = 1.09$ eV, and $E_{ads}(Co) = 1.59$ eV, are also substantially smaller than the adsorption energies on BGDY given in Table 1. The large adsorption binding energies of V, Co and Pd atoms on BGDY are important for single atom catalysis. However, as a second requirement, diffusion and aggregation should be avoided. Diffusion will be studied in the next Section.

The relation between magnetism and catalysis is known since long [40–46], and magnetic nanoparticles have been employed in many industrial reactions [44]. Magnetic ordering in the catalyst sometimes plays a role in the elementary steps of chemical reactions. As a typical example, the methanation reaction on sintered Ni catalysts supported on Al_2O_3 is sensitive to the magnetic-structure [43]. Changes in magnetic ordering at the Curie and Néel temperatures lead to changes in the activity of ferromagnetic and antiferromagnetic catalysts [41]. Also, the magnetic moments of Pd clusters change as a result of adsorption of hydrogen [47]. For these reasons we report in Tables 3 and 4 the values of the total magnetization. In the case of single V, Co and Pd atoms adsorbed on BGDY (Table 4) the magnetic moments are 3, 1 and 0 μ_B per cell, respectively.

4. Metal dimers on the BGDY surface

Adding more metal atoms can lead to formation of an adsorbed cluster or to adsorption of separated atoms (decoration). To compare decoration of the BGDY surface with formation of adsorbed clusters, we have studied the addition of a second atom on the same unit cell. Dimerization and decoration can be compared by calculating the adsorption energy corresponding to the addition of the second atom to the configuration with one metal atom already adsorbed. That is,

$$E_{add\text{ - }dimer} = E\,(M_1@BGDY) + E\,(M_1) - E\,(M_2@BGDY) \quad (3)$$

$$E_{add\text{ - }decor} = E\,(M_1@BGDY) + E\,(M_1) - E\,(2M@BGDY), \quad (4)$$

where all the energies in these two equations have been introduced above, except E(2 M@BGDY), which is the energy of the system formed by two metal atoms adsorbed on different regions of the BGDY unit cell.

The structures obtained for dimerization and decoration are shown in Fig. 4. When a second V atom is added, dimerization and decoration energies (Eqs. (3) and (4)), are 3.63 eV and 2.89 eV, respectively, and dimerization is preferred. It should be noticed that the adsorption energy of the second V atom in the decoration mode, 2.89 eV, is smaller than the adsorption energy of the first one, 3.34 eV in Table 1. This occurs because the presence of the first atom affects the electronic structure of the BGDY substrate. The difference between the adsorption energies of the second atom corresponding to dimerization and decoration modes is 0.74 eV, and this extra binding is a result of a delicate balance between competing effects. The favorable effect is the V-V interaction. But the binding energy of the V_2 dimer in the gas phase is

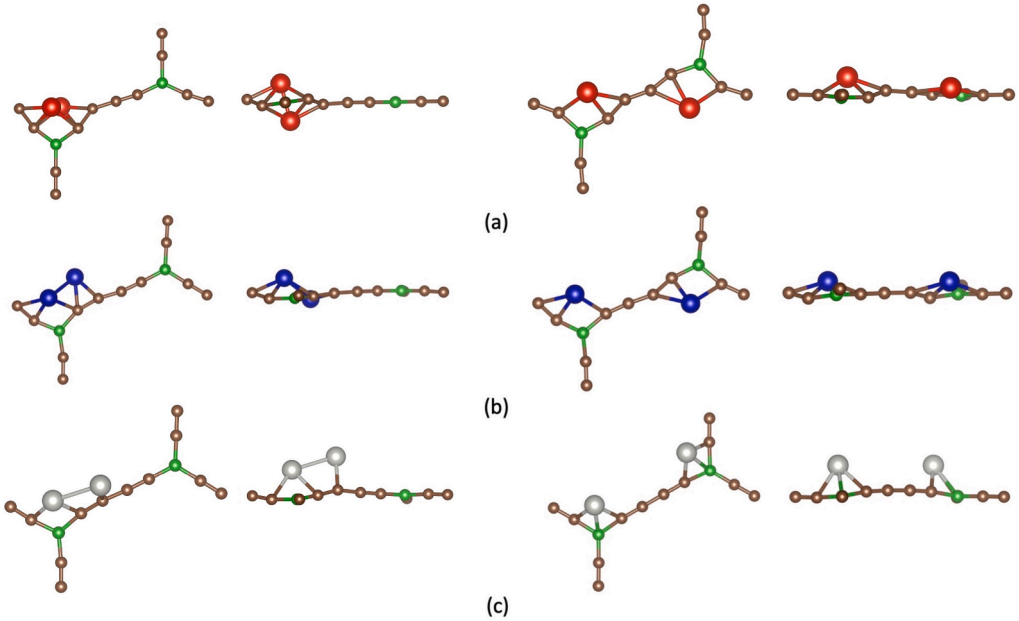

Fig. 4. Lowest energy structures of M_2@BGDY (dimerization), left panels, and 2 M@BGDY (decoration), right panels, for (a) vanadium, (b) cobalt, and (c) palladium. Top and side views are shown in all cases.

Table 5
Bond lengths (in Å) in free and adsorbed metal dimers.

	d(V-V)	d(Co-Co)	d(Pd-Pd)
Free dimer	1.768	1.950	2.418
Adsorbed dimer	2.112	2.235	2.632

2.75 eV [48], and this value is substantially larger than 0.74 eV. The unfavorable contribution comes from the distortion of the BGDY structure to accommodate the two V atoms in the same region of the BGDY, and also from the fact that the bonding capacity of the C1-B-C1 corner is already partially exhausted by the bonding of the first V atom.

Dimerization is also preferential for Co, with the adsorption energies of the second Co atom being 2.89 eV for dimerization and 2.59 eV for decoration. The extra binding, 0.30 eV, is lower than for V. For a second Pd atom, dimerization is slightly preferential over decoration, with energies of 2.45 eV and 2.34 eV, respectively, leading to a difference of 0.11 eV between the two adsorption modes. In the decoration mode, the two atoms prefer to be on the same side of the BGDY layer (the upper

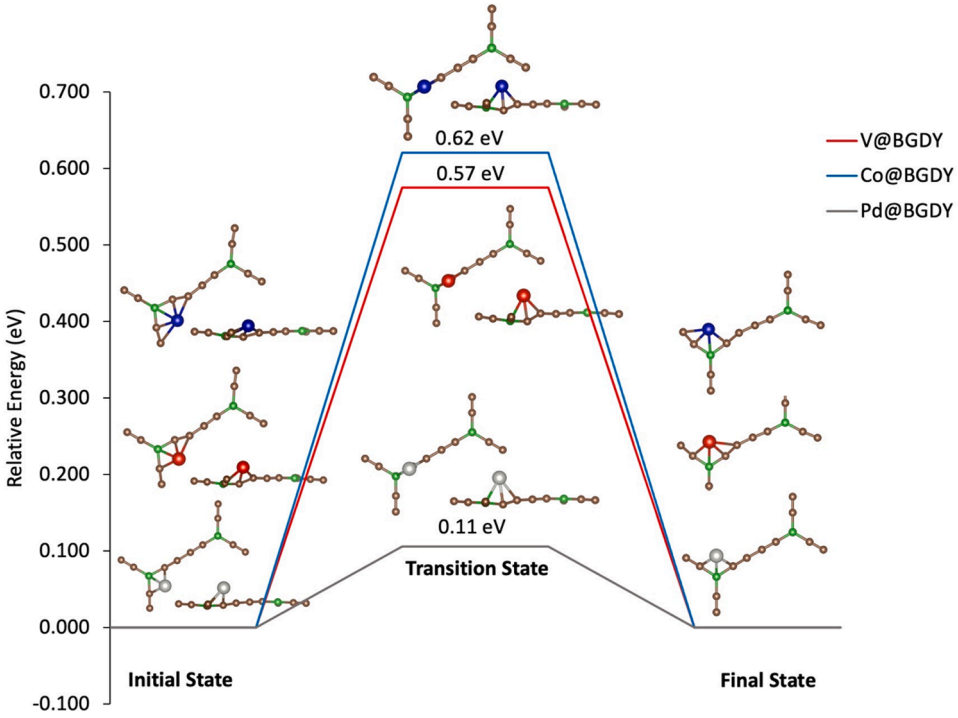

Fig. 5. Energies of the initial, transition and final states for migration of a metal atom from its position on a C1-B-C1 corner to an equivalent position at the closest corner of an adjacent hexagonal hole. The energies of the initial states are aligned at zero energy.

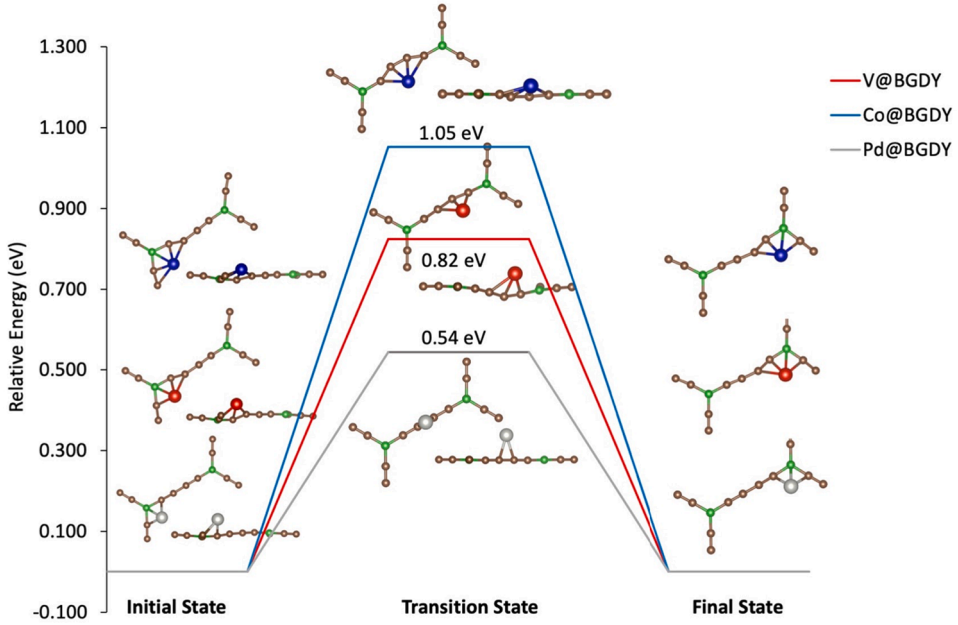

Fig. 6. Energies of the initial, transition and final states for migration of a metal atom from its position on a C1-B-C1 corner to an equivalent position at the closest corner in the same hexagonal hole. The energies of the initial states are aligned at zero energy.

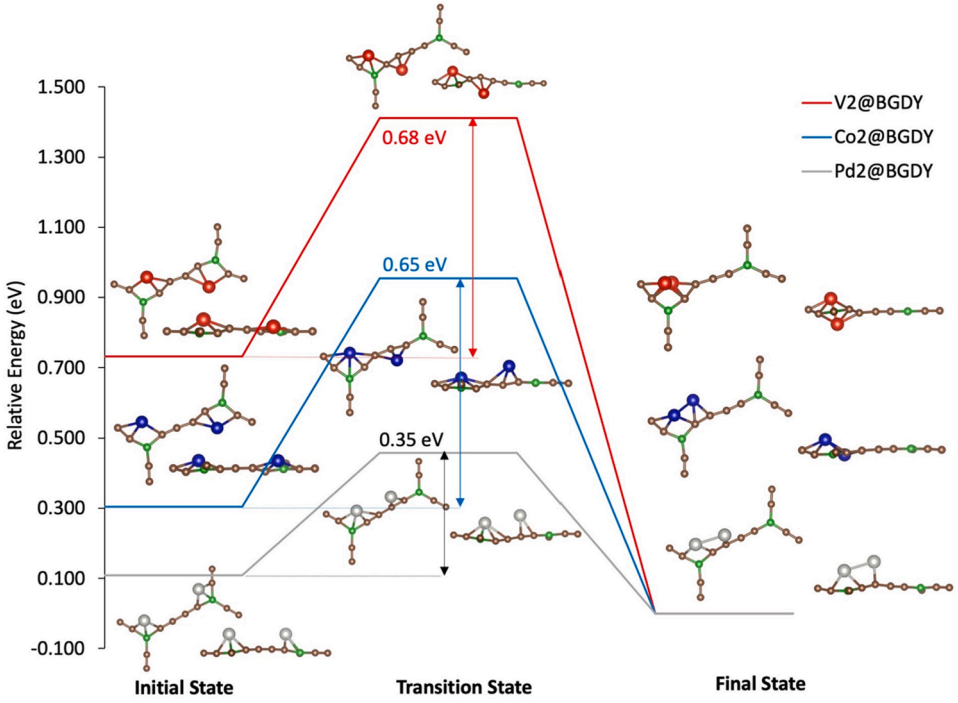

Fig. 7. Energies of the initial, transition and final states for migration of a metal atom from an initial decoration configuration to a final, more stable, dimer configuration. The energies of the final states are aligned at zero energy.

side, in the orientation used in Fig. 4), independently of the metal (V, Co, and Pd). For dimerization, the dimer axis is nearly parallel to the BGDY layer in the case of Pd_2, while in the other two cases the axis is oblique with respect to the BGDY layer, and the second atom is either on the other side of the layer with respect to the first one (this occurs for V_2) or integrated on the layer plane (Co_2).

Because dimerization is preferred over decoration, Table 4 includes the net adsorption energies corresponding to the process of depositing V_2, Co_2 and Pd_2 dimers on the BGDY surface, calculated from Eq. (1). Comparing adsorption energies of Pd_2 on BGDY and other substrates (Table 3), the same trend is observed as for the adsorption of a single atom. The dimer bond lengths, given in Table 5, increase when the dimers are adsorbed, because of the interaction with BGDY, and the bond is highly stretched.

Dimerization might perturb single-atom catalysis if diffusion of the metal atoms through the BGDY surface is possible. Different diffusion paths have been analyzed, and the most relevant ones are discussed now. In the easiest diffusion path, given schematically in Fig. 5, the metal atom, initially in its most stable position on a C1-B-C1 corner, migrates to an equivalent site on the nearest C1-B-C1 corner of an adjacent hexagon. The maximum of the barrier (saddle point) occurs when the metal atom passes on top of one C atom of the C chain, the C atom neighbor to the B atom. The barrier heights, in order of increasing energy, are 0.11, 0.57 and 0.62 eV for Pd, V and Co, respectively. These values correlate with the height z of the metal atom above the BGDY plane in the initial site: the largest value of z occurs for Pd, and the barrier is the lowest. For V and Co, the distance z to the BGDY plane in the initial state is smaller. Then, the atoms have to climb over the carbon chain in order to migrate to the adjacent hexagon, distorting more the substrate (compared to Pd) and giving rise to higher barriers. On the

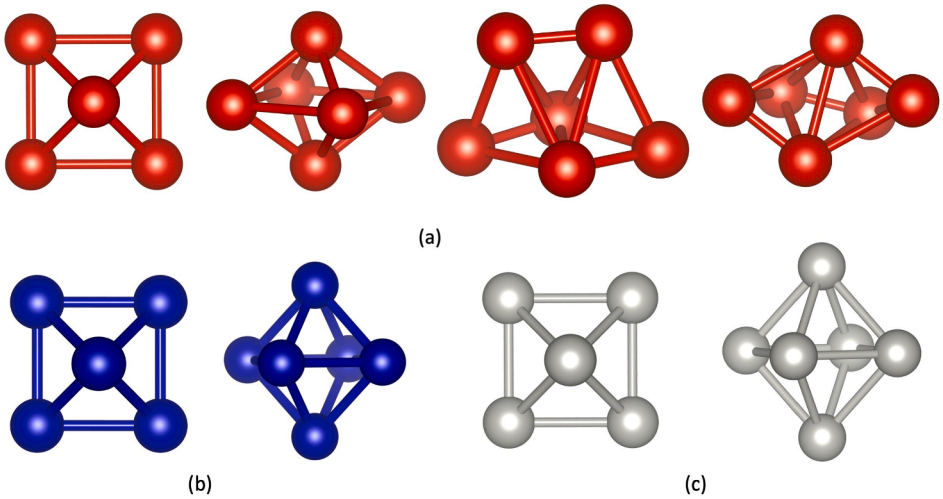

Fig. 8. Top and lateral views of the lowest energy structures of free V_6 (a), Co_6 (b), and Pd_6 (c) clusters. A near degenerate structure (incomplete pentagonal bipyramid) of V_6 is also shown.

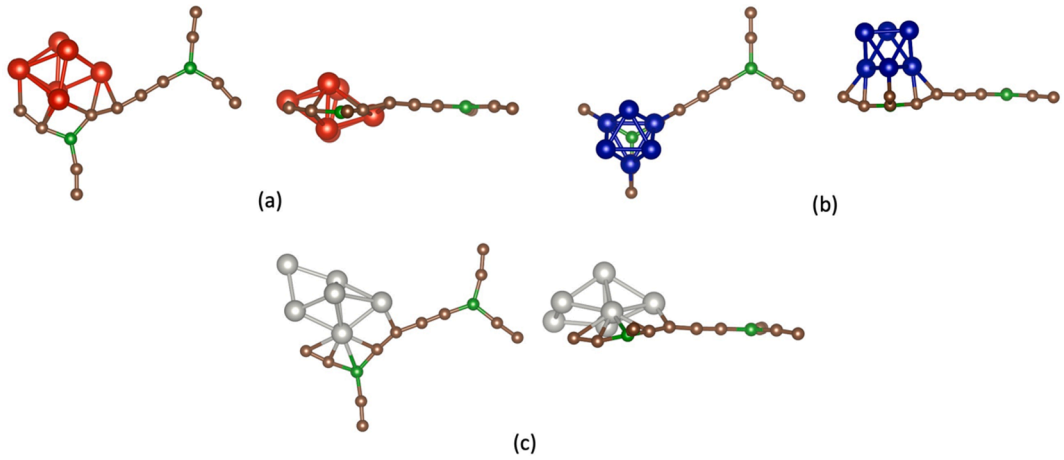

Fig. 9. Lowest energy configurations for the adsorption of (a) V_6, (b) Co_6 and (c) Pd_6 on the BGDY surface. Top (left) and side (right) views are presented.

other hand, migrating to other sites on the same hexagon is more difficult with substantial barrier heights of 0.82 and 1.05 eV for V and Co, respectively. In the diffusion path of Fig. 6, the metal atom migrates from its lowest energy position on a C1-B-C1 corner to the closest corner in the same hexagonal hole. The metal atom approaches the carbon chain and moves approximately parallel to the chain. Again, the barriers for V and Co are larger than the barrier for Pd. In summary, the activation barriers for V and Co atoms are higher compared to Pd, and diffusion at room temperature is expected to be more difficult.

Other relevant events correspond to the migration of one metal atom from its original corner site to another corner which is already occupied by a previously adsorbed metal atom. This is the case for the pass from the decorated configurations to the dimerized configurations in Fig. 4. The calculated diffusion paths, given schematically in Fig. 7, show barriers of height 0.68 eV (V), 0.65 eV (Co) and 0.35 eV (Pd). All the barriers are lowered in comparison to those in Fig. 6 by amounts between 17 and 38%, and this is due to the presence of the previously adsorbed atom. Again, the smallest barrier occurs for the diffusion of the Pd atom, because its height z above the BGDY plane in the initial state is the largest. As shown in Figs. 4 and 7, the two V (or Co) atoms sit on different hexagons in the initial state, and the diffusing atom has to cross the carbon chain to form the dimer: Co crosses the carbon chain from above and V from below in the orientation shown in Fig. 7. Taking together the results of Figs. 5, 6 and 7, one can conclude that atom diffusion at room temperature cannot be neglected for single atom catalysis on this substrate.

5. Metal hexamers on the BGDY surface

After the preferential adsorption sites for one and two atoms have been identified and the tendency for clustering has been confirmed (clustering of transition metals on the surface of graphene, C_{60} and carbon nanotubes has also been predicted [49–51]), the adsorption of M_6 clusters on the BGDY surface has been studied. Hexamers represent a typical example of small clusters used in the laboratory to study catalytic processes [52–54]. First, we have optimized the structures of the isolated clusters. In the three cases, V_6, Co_6 and Pd_6, the lowest energy structure is a distorted octahedron, shown in Fig. 8. The distortion is quite small in Co_6 and Pd_6, and larger in V_6. The distorted V_6 octahedron is, in fact, a square bipyramid in which all the V-V bond lengths between atoms forming the equatorial plane are equal to 2.60 Å, and the V-V distances between equatorial and apex atoms are 2.28 Å. The binding energy per atom is 2.614 eV and the magnetic moment is zero. An isomer near degenerate in energy was found, whose total energy is only 0.010 eV above the square bipyramid. Its structure is an incomplete pentagonal bipyramid (in which one atom is missing in the equatorial plane; this structure is obtained by stretching one of the V-V bonds of the equatorial plane), and the magnetic moment is $\mu = 2\ \mu_B$. The binding energy of Co_6 is 2.938 eV/atom and the Co-Co bond distances vary between 2.257 and 2.264 Å. The binding energy per atom of Pd_6 is 1.973 eV, and the Pd-Pd bond distances form two groups with values 2.604 and 2.690 Å. The total magnetizations of V_6, Co_6 and Pd_6 are 0, 14 and 2 μ_B, respectively. These results are in agreement with previous works for V_6 [55–57], Co_6 [58,59] and Pd_6 [60].

Table 6
Shortest Interatomic distances (in Å) between: 1) metal atoms of the adsorbed hexamer cluster and the boron atom, d(M-B); 2) metal atoms of the cluster and carbon atoms of BGDY, d(M-C). In most cases, a range of values is given.

Distances	V_6-BGDY	Co_6-BGDY	Pd_6-BGDY
d(M-B)	2.435	2.352–2.374	2.355
d(M-C)	2.003–2.233	1.918–2.018	2.039–2.198

Based on the information on the structures of free M_6 clusters, we can study their adsorption on BGDY. Different locations were investigated. Adsorption locations near the C1-B-C1 corner (see Fig. 1) were explored, motivated by the previous results for the adsorption of single atoms and dimers. Also, other possible configurations have been investigated: the cluster on top of the B atom, the cluster in the central region of the hexagonal holes, and near the carbon chains. In all cases, the metal atoms and the atoms of the substrate are allowed to move and optimize their positions in order to reach the lowest energy configuration. The results for the most stable structures are collected in Fig. 9. An extended view of the structures, including several cells of the periodic calculation, is given in Figure S1 of the Supplementary Material. The shortest distances between metal and carbon atoms, and between boron and metal atoms, are given in Table 6. In most cases, a range of values is provided because there are several interatomic distances with close values. The most favorable position of V_6, shown in Fig. 9 (a), is on the hexagonal hole corner. The V_6 square bipyramid is oriented such that its equatorial plane is perpendicular to the BGDY layer. The two V-V edges of the equatorial plane which are perpendicular to the BGDY layer have one V atom above and one below the layer, and the two apical V atoms of the bipyramid fit in the BGDY plane. The shortest interatomic distances between V atoms and C atoms vary between 2.003 and 2.233 Å. Because of the interaction between V_6 and BGDY, the layer becomes distorted, and the V-V bond lengths change a bit compared to free V_6. The adsorption energy, obtained from Eq. (1), is 6.26 eV, and the total magnetization is 2 μ_B per cell.

The most stable adsorbed geometry of the Co_6 cluster, on top of the B atom, is shown in Fig. 9 (b). The adsorption energy of Co_6 is 4.12 eV, a smaller value compared to V_6. One triangular face of the Co_6 octahedron

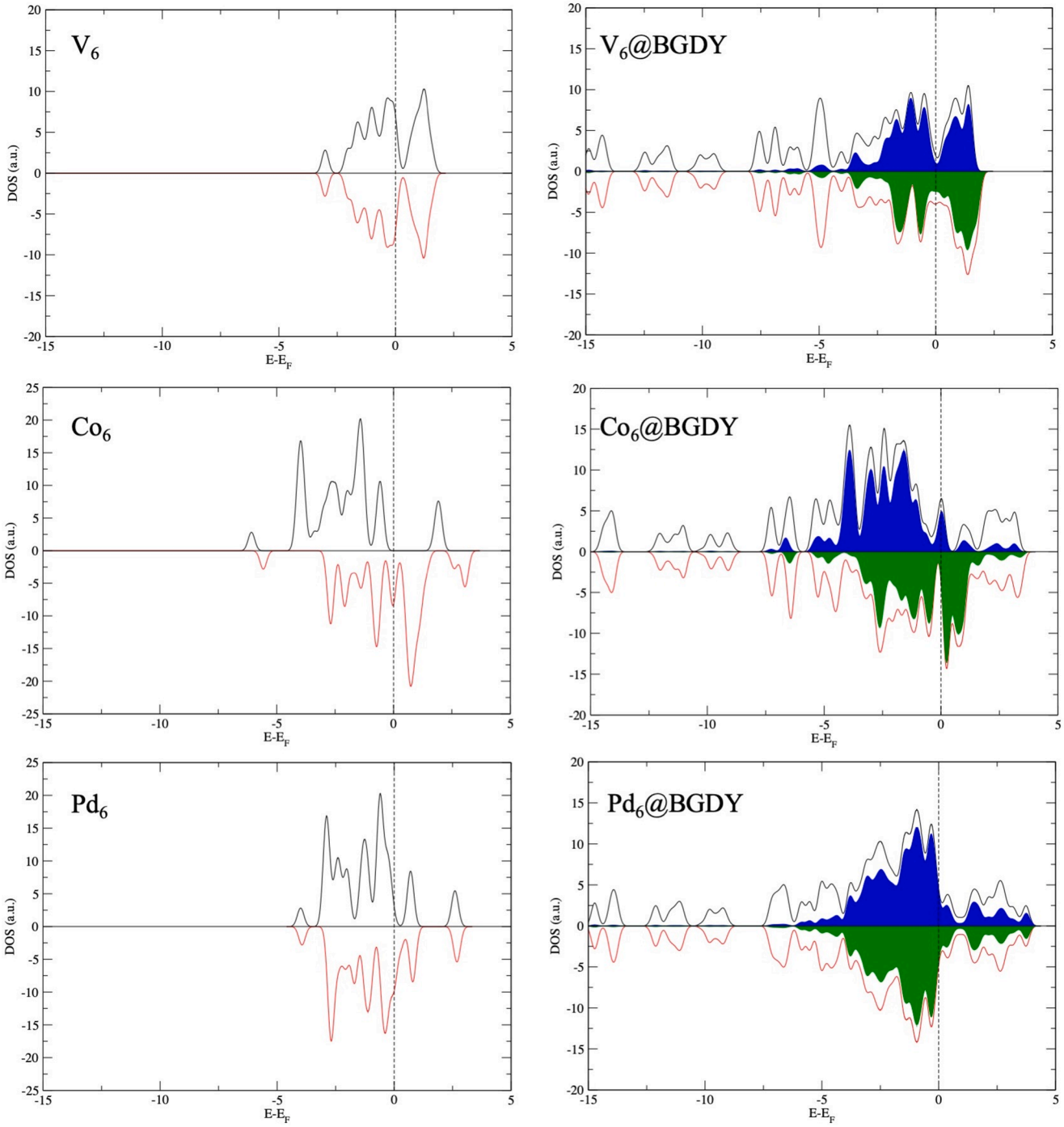

Fig. 10. Density of electronic states (DOS) of free M_6 and M_6@BGDY, M = V, Co, Pd. Spin up and spin down DOS are indicated by the black and red curves, respectively. Energies are measured with respect to the Fermi energy. In the case of the supported clusters, the spin up and spin down DOS projected on the metal are plotted in blue and green colors, respectively. (For interpretation of the references to colour in this figure legend, the reader is referred to the web version of this article.)

is located on top of the B atom and parallel to the BGDY layer. Those three Co atoms interact directly with C atoms of BGDY, and the interaction distorts slightly the geometry of Co_6. The total magnetization of this system is 10 μ_B per cell. Adsorption of Pd_6 occurs on the hexagonal hole corner. The original octahedral structure of Pd_6 changes to form a capped trigonal bipyramid with the capping Pd atom bonded in a bridge position to the two atoms of a Pd-Pd edge. Four Pd atoms interact with the BGDY surface. The adsorption energy of Pd_6 is 4.21 eV, and the system has zero net magnetization. Comparison with the adsorption energies of Pd_6 on other substrates (given in Table 3) reveals the same trend shown by the adsorption of Pd and Pd_2. The magnetic moment of a free Pd atom is zero, and this is also its value when the atom is adsorbed, independent of the substrate (see Table 3). The magnetic moments of the free dimer and hexamer are $\mu = 2\ \mu_B$. Adsorption quenches the magnetic moments with the exception of Pd_6 on graphene [37]. The shortest metal-boron distances do not show a clear trend, and this is a result of the different adsorption configurations: on the hexagonal hole corner for V_6 and Pd_6, and on top of the B atom in the case of Co_6.

The analysis of the density of electronic states (DOS) helps interpreting the adsorption binding energies of the clusters and the changes

in the magnetic moments between free and adsorbed clusters. BGDY is a semiconductor with a moderate band gap [13,14,16,17]. Fig. 10 shows a comparison of the DOS of free V_6, Co_6 and Pd_6 with those of V_6@BGDY, Co_6@BGDY and Pd_6@BGDY. Spin up and spin down DOS are shown as black and red curves, respectively. The DOS of V_6 shows a perfect compensation between spin up and spin down electronic states, consistent with the magnetic moment μ (freeV_6) = 0. On the other hand, the DOS of the system V_6@BGDY reveals a small energy shift between the spin up and spin down states which is responsible of the magnetic moment μ (V_6@BGDY) = 2 μ_B per cell. The spin up and spin down DOS projected on V_6, plotted in blue and green colors, respectively, reveal that the relative energy shift arises from those states; in particular, from the states with binding energies less than 3.5 eV. The magnetic instability inherent to the large DOS at the Fermi energy in free V_6 is lifted up by the interaction with BGDY, resulting in the relative shift between spin up and spin down states, and in a lowering of the energy of V_6@BGDY. The total and projected DOS of V_6@BGDY reveal a substantial energy overlap -and interaction- between the V_6 and BGDY states which is responsible of the large bonding energy (6.26 eV) between V_6 and the BGDY substrate. Also, in the cases of Co_6 and Pd_6 the interaction between metal and substrate electronic states is substantial, accounting for the large adsorption energies (4.12 eV for Co_6 and 4.21 eV for Pd_6). The DOS of free Co_6 shows a large shift between spin up and spin down states, responsible for the large magnetic moment μ (free Co_6) = 14 μ_B. The interaction with BGDY moves some spin up states towards the Fermi energy, and at the same time stabilizes a bit the spin down states, resulting in a reduction of the value of the magnetic moment to μ (Co_6@BGDY) = 10 μ_B. The DOS of free Pd_6 shows a shift between spin up and spin down states, responsible for the magnetic moment μ (free Pd_6) = 2 μ_B, and the interaction with BGDY completely quenches the magnetic moment. The same is observed for Pd_6 adsorbed on a graphene vacancy [38] and on GDY [34].

6. Summary and conclusions

Layered carbon materials can be useful as supports for catalytic metallic nanoparticles in the anode of fuel cells, and in other applications. Also, doping layered and porous carbons with metal atoms and nanoparticles is known to enhance the hydrogen storage capacity of those materials. For these reasons, using the density functional theory we have investigated the adsorption of transition metal atoms, vanadium, cobalt and palladium, and small clusters, on a novel layered material recently synthesized: boron graphdiyne. This layered material contains uniformly distributed holes that can host the metal clusters. Single V, Co and Pd atoms sit at the corners of the structure, near the boron atoms, and slightly above the BGDY plane. Their binding energies are large enough to make the systems apt for single-atom catalysis, but diffusion cannot be overlooked. The adsorption binding energies of the single atoms on BGDY are substantially larger than on pristine graphene. Dimer (V_2, Co_2, Pd_2) formation on BGDY is energetically preferred over adsorption of two separated atoms (decoration). The dimers occupy positions near the corners, with the dimer axis of Pd_2 nearly parallel to the BGDY, and forming an angle with the BGDY plane for V_2 and Co_2. In the case of hexamer adsorption, differences occur between V_6, Co_6 and Pd_6. The octahedral structure of free Co_6 is preserved on adsorption, which takes place on top of a boron atom. V_6 is adsorbed on the C-B-C corners, and the square bipyramid structure of free V_6 is maintained on adsorption. Adsorption of Pd_6 also occurs on the corners of the hollow BGDY, but the octahedral structure of the free cluster changes. The binding energies of the V_6, Co_6 and Pd_6 clusters to the substrate are sufficiently large to become tightly anchored. Comparison with previous work on other substrates is possible for Pd, and in the three cases analyzed (single atom, dimer and hexamer) the binding energies on BGDY are substantially larger than on pristine graphene, similar to the binding energies on GDY and smaller than the binding energies on a graphene vacancy. Adsorption of the hexamers still leaves a lot of empty space in the hexagonal holes of BGDY, and anchoring of larger metal clusters should be possible. The large adsorption binding energies, combined with the presence of pores in the layer, make BGDY a promising synthetic filtrating membrane for the separation of metals in water or other liquids.

CRediT authorship contribution statement

Estefanía Germán: Conceptualization, Methodology, Software, Investigation, Formal analysis, Writing - original draft, Writing - review & editing, Visualization, Funding acquisition. **Ana Alvarez-Yenes:** Methodology, Investigation, Visualization. **Julio A. Alonso:** Conceptualization, Supervision, Investigation, Formal analysis, Writing - original draft, Writing - review & editing, Funding acquisition. **María J. López:** Conceptualization, Supervision, Investigation, Formal analysis, Writing - original draft, Writing - review & editing, Funding acquisition.

Declaration of Competing Interest

The authors declare that they have no known competing financial interests or personal relationships that could have appeared to influence the work reported in this paper.

Acknowledgments

Work supported by Junta de Castilla y León (Grant VA021G18), Ministerio de Ciencia e Innovación of Spain (Project PID2019-104924RB-I00) and University of Valladolid (GIR Nanostructure Physics). Estefanía German acknowledges a postdoctoral contract with University of Valladolid. The authors thankfully acknowledge the facilities provided by Centro de Proceso de Datos-Parque Científico (University of Valladolid). We also acknowledge Dr. Tanveer Hussain for useful comments.

Appendix A. Supplementary data

Supplementary data to this article can be found online at https://doi.org/10.1016/j.apsusc.2021.149270.

References

[1] R. Hoffmann, A. Kabanov, A. Golov, D. Proserpio, Homo citans and carbon allotropes: for an ethics of citation, Angew. Chemie 55 (2016) 10962–10976, https://doi.org/10.1002/anie.201600655.
[2] K.S. Novoselov, A.K. Geim, S.V. Morozov, D. Jiang, Y. Zhang, S.V. Dubonos, I. V. Grigorieva, A.A. Firsov, Electric field effect in atomically thin carbon films, Science 306 (2004) 666–669, https://doi.org/10.1126/science.1102896.
[3] G.W. Flynn, Perspective: the dawning of the age of graphene, J. Chem. Phys. 135 (2011) 050901, https://doi.org/10.1063/1.3615063.
[4] Y. Cao, V. Fatemi, S. Fang, K. Watanabe, T. Taniguchi, E. Kaxiras, P. Jarillo-Herrero, Unconventional superconductivity in magic-angle graphene superlattices, Nature 556 (2018) 43–50, https://doi.org/10.1038/nature26160.
[5] W. Choi, I. Lahiri, R. Seelaboyina, Y.S. Kang, Synthesis of graphene and its applications: a review, Crit. Rev. Solid State Mater. Sci. 35 (2010) 52–71, https://doi.org/10.1080/10408430903505036.
[6] G. Li, Y. Li, H. Liu, Y. Guo, Y. Li, D. Zhu, Architecture of graphdiyne nanoscale films, Chem. Commun. 46 (2010) 3256–3258, https://doi.org/10.1039/B922733D.
[7] H. Bu, M. Zhao, H. Zhang, X. Wang, Y. Xi, Z. Wang, Isoelectronic doping of graphdiyne with boron and nitrogen: stable configurations and band gap modification, J. Phys. Chem. A 116 (2012) 3934–3939, https://doi.org/10.1021/jp300107d.
[8] C. Sun, D.J. Searles, Lithium storage on graphdiyne predicted by DFT calculations, J. Phys. Chem. C 116 (2012) 26222–26226, https://doi.org/10.1021/jp309638z.
[9] X. Qian, H. Liu, C. Huang, S. Chen, L. Zhang, Y. Li, J. Wang, Y. Li, Self-catalyzed growth of large-area nanofilms of two-dimensional carbon, Sci. Rep. 5 (2015) 7756, https://doi.org/10.1038/srep07756.
[10] H.J. Hwang, Y. Kwon, H. Lee, Thermodynamically stable calcium-decorated graphyne as a hydrogen storage medium, J. Phys. Chem. C 116 (2012) 20220–20224, https://doi.org/10.1021/jp306222v.
[11] C. Huang, S. Zhang, H. Liu, Y. Li, G. Cui, Y. Li, Graphdiyne for high capacity and long-life lithium storage, Nano Energy 11 (2015) 481–489, https://doi.org/10.1016/j.nanoen.2014.11.036.

[12] S.W. Cranford, M.J. Buehler, Selective hydrogen purification through graphdiyne under ambient temperature and pressure, Nanoscale 4 (2012) 4587–4593, https://doi.org/10.1039/C2NR30921A.

[13] N. Wang, X. Li, Z. Tu, F. Zhao, J. He, Z. Guan, C. Huang, Y. Yi, Y. Li, Synthesis, electronic structure of boron–graphdiyne with an sp-hybridized carbon skeleton and its application in sodium storage, Angew. Chem. 57 (2018) 3968–3973, https://doi.org/10.1002/anie.201800453.

[14] B. Mortazavi, M. Shahrokhi, X. Zhuang, T. Rabczuk, Boron–graphdiyne: a superstretchable semiconductor with low thermal conductivity and ultrahigh capacity for Li, Na and Ca ion storage, J. Mater. Chem. A 6 (2018) 11022–11036, https://doi.org/10.1039/C8TA02627K.

[15] I. Muhammad, S. Wang, J. Liu, H. Xie, Q. Sun, Boron-graphdiyne as an anode material for Li, Na, and K ion batteries with high capacities and low diffusion barriers, J. Renew. Sustainable Energy 11 (2019) 014106, https://doi.org/10.1063/1.5079928.

[16] H. Wang, Y. Gao, Q. Li, J. Zhao, Electronic structures and charge carrier mobilities of boron-graphdiyne sheet and nanoribbons, Physica E 124 (2020) 114354, https://doi.org/10.1016/j.physe.2020.114354.

[17] T. Hussain, B. Mortazavi, H. Bae, T. Rabczuk, H. Lee, A. Karton, Enhancement in hydrogen storage capacities of light metal functionalized boron-graphdiyne nanosheets, Carbon 147 (2019) 199–205, https://doi.org/10.1016/j.carbon.2019.02.085.

[18] C.I. Contescu, C.M. Brown, Y. Liu, V.V. Bhat, N.C. Gallego, Detection of hydrogen spillover in palladium modified activated carbon fibers during hydrogen adsorption, J. Phys. Chem. C 113 (2009) 5886–5890, https://doi.org/10.1021/jp900121k.

[19] V.V. Bhat, C.I. Contescu, N.C. Gallego, F.S. Baker, Atypical hydrogen uptake on chemically-activated, ultramicroporous carbon, Carbon 48 (2010) 1331–1340, https://doi.org/10.1016/j.carbon.2009.12.001.

[20] C.I. Contescu, K. van Benthem, S. Li, C.S. Bonifacio, S.J. Pennycook, P. Jena, N. C. Gallego, Single Pd atoms in activated carbon fibers and their contribution to hydrogen storage, Carbon 49 (2011) 4050–4058, https://doi.org/10.1016/j.carbon.2011.05.021.

[21] I.C. Gerber, P. Serp, A theory/experience description of support effects in carbon-supported catalysts, Chem. Rev. 120 (2020) 1250–1349, https://doi.org/10.1021/acs.chemrev.9b00209.

[22] A. Wang, J. Li, T. Zhang, Heterogeneous single-atom catalysis, Nat. Rev. Chem. 2 (2018) 65–81, https://doi.org/10.1038/s41570-018-0010-1.

[23] P. Giannozzi, S. Baroni, N. Bonini, M. Calandra, R. Car, C. Cavazzoni, D. Ceresoli, G. L. Chiarotti, M. Cococcioni, I. Dabo, et al., QUANTUM ESPRESSO: a modular and open-source software project for quantum simulations of materials, J. Phys.: Condens. Matter, 21 (2009) 395502 19pp. https://doi:10.1088/0953-8984/21/39/395502.

[24] J.P. Perdew, K. Burke, M. Ernzerhof, Generalized gradient approximation made simple, Phys. Rev. Lett. 77 (1996) 3865–3868, https://doi.org/10.1103/PhysRevLett.77.3865.

[25] B. Hammer, L.B. Hansen, J.K. Nørskov, Improved adsorption energetics within density-functional theory using revised Perdew-Burke-Ernzerhof functionals, Phys. Rev. B 59 (1999) 7413–7421, https://doi.org/10.1103/PhysRevB.59.7413.

[26] G. Kresse, D. Joubert, From ultrasoft pseudopotentials to the projector augmented-wave method, Phys. Rev. B 59 (1999) 1758–1775, https://doi.org/10.1103/PhysRevB.59.1758.

[27] P.E. Blöchl, Projector augmented-wave method, Phys. Rev. B 50 (1994) 17953–17979, https://doi.org/10.1103/PhysRevB.50.17953.

[28] http://www.quantum-espresso.org/pseudopotentials/.

[29] H.J. Monkhorst, J.D. Pack, Special points for Brillouin-zone integrations, Phys. Rev. B 13 (1976) 5188–5192, https://doi.org/10.1103/PhysRevB.13.5188.

[30] S. Grimme, J. Antony, S. Ehrlich, H. Krieg, A consistent and accurate ab initio parametrization of density functional dispersion correction (DFT-D) for the 94 elements H-Pu, J. Chem. Phys. 132 (2010) 154104, https://doi.org/10.1063/1.3382344.

[31] G. Henkelman, B.P. Uberuaga, H. Jónsson, A climbing image nudged elastic band method for finding saddle points and minimum energy paths, J. Chem. Phys. 113 (2000) 9901–9904, https://doi.org/10.1063/1.1329672.

[32] S. Gong, Q. Wang, Boron-doped graphene as a promising anode material for potassium-ion batteries with a large capacity, high rate performance, and good cycling stability, J. Phys. Chem. C 121 (2017) 24418–24424, https://doi.org/10.1021/acs.jpcc.7b07583.

[33] Z. Xu, X. Lv, J. Li, J. Chen, Q. Liu, A promising anode material for sodium-ion battery with high capacity and high diffusion ability: Graphyne and graphdiyne, RSC Adv. 6 (2016) 25594–25600, https://doi.org/10.1039/C6RA01870J.

[34] A. Seif, M.J. López, A. Granja-Del Rio, K. Azizi, J.A. Alonso, Adsorption and growth of palladium clusters on graphdiyne, Phys. Chem. Chem. Phys. 19 (2017) 19094–19102, https://doi.org/10.1039/c7cp03263c.

[35] J. Rogan, G. García, J.A. Valdivia, W. Orellana, A.H. Romero, R. Ramírez, M. Kiwi, Small Pd clusters: a comparison of phenomenological and ab initio approaches, Phys. Rev. B 72 (2005) 115421, https://doi.org/10.1103/PhysRevB.72.115421.

[36] K.T. Chan, J.B. Neaton, M.L. Cohen, First-principles study of metal adatom adsorption on graphene, Phys. Rev. B 77 (2008) 235430, https://doi.org/10.1103/PhysRevB.77.235430.

[37] I. Cabria, M.J. López, S. Fraile, J.A. Alonso, Adsorption and dissociation of molecular hydrogen on palladium clusters supported on graphene, J. Phys. Chem. C 116 (2012) 21179–21189, https://doi.org/10.1021/jp305635w.

[38] M.J. López, I. Cabria, J.A. Alonso, Palladium clusters anchored on graphene vacancies and their effect on the reversible adsorption of hydrogen, J. Phys. Chem. C 118 (2014) 5081–5090, https://doi.org/10.1021/jp410262t.

[39] H. Valencia, A. Gil, G. Frapper, Trends in the adsorption of 3d transition metal atoms onto graphene and nanotube surfaces: a DFT study and molecular orbital analysis, J. Phys. Chem. C 114 (2010) 14141–14153, https://doi.org/10.1021/jp103445v.

[40] P.W. Selwood, Magnetism and catalysis, Chem. Rev. 38 (1946) 41–82, https://doi.org/10.1021/cr60119a002.

[41] R.J.H. Voorhoeve, Experimental relationships between catalysis and magnetism, AIP Conf. Proceedings 18 (1974) 19–32, https://doi.org/10.1063/1.2947317.

[42] J.T. Richardson, Magnetism and catalysis, J. Appl. Phys. 49 (1978) 1781–1786, https://doi.org/10.1063/1.324865.

[43] R.C. Everson, L.N. Mulay, O.P. Mahajan, P.L. Walker, Magnetic and catalytic properties of sintered nickel catalysts for the methanation reaction, J. Chem. Technol. Biotechnol. 29 (1979) 1–7, https://doi.org/10.1002/jctb.503290102.

[44] Y. Zhu, L.P. Stubbs, F. Ho, R. Liu, C.P. Ship, J.A. Maguire, N.S. Hosmane, Magnetic nanocomposites: a new perspective in catalysis, CatChemCat 2 (2010) 365–374, https://doi.org/10.1002/cctc.200900314.

[45] L.M. Rossi, N.J.S. Costa, F.P. Silva, R. Wojcieszak, Magnetic nanomaterials in catalysis: advanced catalysts for magnetic separation and beyond, Green Chem. 16 (2014) 2906–2933, https://doi.org/10.1039/C4GC00164H.

[46] J. Ma, C. Liu, K. Chen, Insight in the relationship between magnetism of stoichiometric spinel ferrites and their catalytic activity, Catal. Commun. 140 (2020) 105986, https://doi.org/10.1016/j.catcom.2020.105986.

[47] M.J. López, M. Blanco-Rey, J.I. Juaristi, M. Alducin, J.A. Alonso, Manipulating the magnetic moment of palladium clusters by adsorption and dissociation of molecular hydrogen, J. Phys. Chem. C 121 (2017) 20756–20762, https://doi.org/10.1021/acs.jpcc.7b03996.

[48] E.M. Spain, M.D. Morse, Bond strengths of transition-metal dimers: titanium-vanadium (TiV), vanadium dimer, titanium-cobalt (TiCo), and vanadium-nickel (VNi), J. Phys. Chem. 96 (1992) 2479–2486, https://doi.org/10.1021/j100185a018.

[49] I. Cabria, M.J. López, J.A. Alonso, Theoretical study of the transition from planar to three-dimensional structures of palladium clusters supported on graphene, Phys. Rev. B 81 (2010) 035403, https://doi.org/10.1103/PhysRevB.81.035403.

[50] Q. Sun, Q. Wang, P. Jena, Y. Kawazoe, Clustering of Ti on a C_{60} surface and its effect on hydrogen storage, J. Am. Chem. Soc. 127 (2005) 14582–14583, https://doi.org/10.1021/ja0550125.

[51] P.O. Krasnov, F. Ding, A.K. Singh, B.I. Yakobson, Clustering of Sc on SWNT and reduction of hydrogen uptake: Ab-initio all electron calculations, J. Phys. Chem. C 111 (2007) 17977–17980, https://doi.org/10.1021/jp077264t.

[52] S. Lee, L.M. Molina, M.J. López, J.A. Alonso, B. Hammer, B. Lee, S. Seifert, R. E. Winans, J.W. Elam, M.J. Pellin, S. Vajda, Selective propene epoxidation on immobilized Au_{6-10} clusters: te effect of hydrogen and water on activity and selectivity, Angew. Chem. Internat. Edit. 48 (2009) 1467–1471, https://doi.org/10.1002/anie.200804154.

[53] S.M. Lang, T.M. Bernhardt, R.N. Barnett, U. Landman, Size-dependent binding energies of methane to small gold clusters, ChemPhysChem 11 (2010) 1570–1577, https://doi.org/10.1002/cphc.200900844.

[54] S.M. Lang, I. Fleischer, T.M. Bernhardt, R.N. Barnett, U. Landman, Size-dependent self-limiting oxidation of free palladium clusters, J. Phys. Chem. A 118 (2014) 8572–8582, https://doi.org/10.1021/jp502736p.

[55] H. Grönbeck, A. Rosen, Geometric and electronic properties of small vanadium clusters: a density functional study, J. Chem. Phys. 107 (1997) 10620, https://doi.org/10.1063/1.474177.

[56] G. Wu, M. Yang, X. Guo, J. Wang, Comparative DFT study of N_2 and NO adsorption on vanadium clusters V_n (n = 2–13), J. Comput. Chem. 33 (2012) 1854–1861, https://doi.org/10.1063/1.474177.

[57] A. Taneda, T. Shimizu, Y. Kawazoe, Stable disordered structures of vanadium clusters, J. Phys.: Condens. Matter 13 (2001) L305, https://doi.org/10.1088/0953-8984/13/16/101.

[58] A. Sebetci, Cobalt clusters (Co_n, n >= 6) and their anions, Chem. Phys. 354 (2008) 196–201, https://doi.org/10.1016/j.chemphys.2008.10.032.

[59] K. García-Díez, J. Fernández-Fernández, J.A. Alonso, M.J. López, Theoretical study of the adsorption of hydrogen on cobalt clusters, Phys. Chem. Chem. Phys. 20 (2018) 21163–21176, https://doi.org/10.1039/C8CP03048K.

[60] P. Nava, M. Sierka, R. Ahlrichs, Density functional study of palladium clusters, Phys. Chem. Chem. Phys. 5 (2003) 3372–3381, https://doi.org/10.1039/B303347C.